Electronic Supplementary Information

Enhanced Photochemical Effects of Plasmonic Cluster Catalysts through Aggregated Nanostructures

*Xu Hu,[†a] Zhijie Zhu,[†a] Yuxuan Zhou,[†a] Shuang Liu,[a] Chunpeng Wu,[a] Jiaqi Wang,[a] Yihao Sheng,[a] Tianran Yan,[a] Liang Zhang,[a,b] Jinxing Chen,[a,b] Kai Feng,[a,b] Alexander Genest,[c] Günther Rupprechter,[c] Xingda An,[*a,b] Chaoran Li[*a,d] and Le He[*a,b]*

[a] Institute of Functional Nano & Soft Materials (FUNSOM), Soochow University, Suzhou, 215123, Jiangsu, PR China.

[b] Jiangsu Key Laboratory of Advanced Negative Carbon Technologies, Soochow University, Suzhou, 215123, Jiangsu, PR China

[c] Institute of Materials Chemistry, Technische Universität Wien, Vienna 1060, Austria

[d] Jiangsu Key Laboratory for Carbon-Based Functional Materials & Devices, Soochow University, 199 Ren'ai Road, Suzhou, 215123, Jiangsu, PR China.

[†] Authors who equally contribute to the paper.

E-mails: xdan@suda.edu.cn, crli@suda.edu.cn, lehe@suda.edu.cn.

This file includes Experimental Section, Figs. S1-S17 and Tables S1.

Experimental Section

Synthesis of Pt-Cu nanocrystalline cluster aggregates (Pt-Cu CAs)

Pt-Cu bimetallic nanocrystalline cluster aggregates were prepared by a wet-chemical method easily. In a typical synthesis of Pt1-Cu1 CAs, Copper chloride ($CuCl_2$, 6.4 mL, 0.1 mol·L^{-1}) solution, chloroplatinic acid solution (H_2PtCl_6, 6.4 ml, 0.1 mol·L^{-1}) solution and polyvinyl pyrrolidone (PVP, 25 mL, 1g·mL^{-1}) solution were mixed into an ethanol aqueous solution (V ethanol/V water = 50 mL/100 mL) by stirring for 30 min at room temperature. Then, ascorbic acid (AA, 12.5 mL, 1 mol·L^{-1}) solution was added into the mixture. After five minutes of reaction, the products were centrifuged at 11.000 r·min^{-1} for 1 h and washed for 4 times with deionized water.

The bimetallic nanocrystalline cluster aggregates catalysts with different Pt/Cu ratios were synthesized by adjusting the volume ratio of $CuCl_2$ solution and H_2PtCl_6 solution.

Synthesis of Pt-Cu nanoparticles-large (Pt-Cu LPs)

In a typical synthesis of 20 nm Pt1-Cu1 LPs, 0.25 mmol Platinum (II) acetylacetonate ($Pt(acac)_2$, 97%) and 0.25 mmol Copper (II) acetylacetonate ($Cu(acac)_2$, 97%) were mixed with 10 mL of oleylamine ($CH_3(CH_2)_7CH=CH(CH_2)CH_2NH_2$, OAm) and stirred under a gentle flow of N_2 for 40 minutes. The mixture was heated to 300 °C at a heating rate of 4 °C·min^{-1} and held at 300 °C for 60 minutes, then cooled to room temperature. The mixture was then centrifuged at 10.000 rpm for 10 minutes and washed three times with a hexane/ethanol mixture.

The bimetallic nanoparticles catalysts with different Pt/Cu ratios were synthesized by adjusting the mass ratio of $Pt(acac)_2$ and $Cu(acac)_2$.

Synthesis of Pt-Cu nanoparticles-small (Pt-Cu SPs)

In a typical synthesis of 3 nm Pt1-Cu1 SPs, 0.25 mmol $Pt(acac)_2$ and 0.25 mmol $Cu(acac)_2$ were mixed with 30 mL of oleylamine (OAm) and stirred for 40 min under mild N_2 flow. Simultaneously 40 mL of the OAm solution was heated to 210 °C at a heating rate of 4 °C·min^{-1}. 10 mL of the well-stirred mixture solution was injected into the hot OAm solution and kept at 210 °C for 60 min. It was then cooled to room temperature. The solution was then separated by centrifugation at 11.000 rpm for 60 minutes and washed three times with a hexane/ethanol mixture.

The bimetallic nanoparticles catalysts with different Pt/Cu ratios were synthesized by adjusting the mass ratio of $Pt(acac)_2$ and $Cu(acac)_2$.

Catalytic reduction of p-nitrophenol

5 mL of p-nitrophenol solution (p-NP, 10^{-3} mol·L^{-1}) and 5 ml of NaBH$_4$ (0.1 mol·L^{-1}) solution were mixed well in a glass vial. Then, 0.2 ml of the mixture solution were added to a cuvette containing 1.8 ml of deionized water to measure the initial absorption spectra using a UV-vis absorption spectrophotometer. 10ul of 5 mg·ml^{-1} catalyst solution was added to the glass vial for the catalytic reaction. During the reaction, 0.2 mL of the reaction solution was injected into a cuvette with 1.8 ml of deionized water at certain intervals to continue the characterization.

When testing the reduction of p-NP at different reaction concentrations, the ratio of reaction solution to deionized water in the test cuvette needs to be adjusted to ensure that the peak of the absorbance spectral curve is around 1 before reaction.

Photocatalytic reduction of p-nitrophenol

The photocatalytic p-NP reduction reaction was tested as under dark conditions, except that an additional light source was added. Photocatalytic reduction of p-NP over as-prepared samples were carried out under irradiation (Beijing Merry Change, MC23091302) at ambient temperature.

Photoelectrochemical tests

Electrochemical measurements were carried out with a three-electrode system on a CHI 600C electrochemical analyser (CH Instrument, China). A platinum wire, a Ag/AgCl, and a glassy carbon electrode (GCE, 3 mm in diameter) modified by catalyst were used as the counter, reference and working electrode, respectively. The fabrication protocol of the working electrode is as follows: 4 mg of various catalysts powder was dispersed in 1 ml of 3:1 water/ethanol solvent with 40 ul of Nafion solution (5 wt%, Sigma-Aldrich) before being ultrasonicated for 20 min to generate a homogeneous ink.

All photoelectrochemical tests, including CV, LSV, M-S, EIS i-t, etc., were made in the mixture of 0.1 mol·L^{-1} CH$_3$COONa solution and 0.1 mol·L^{-1} p-NP solution. The power density is controlled by the LED driver to be the same. The wavelength dependence test used LEDs with wavelengths of 365, 420, 470, 520, 590, 620, 740 nm; The light intensity dependence test used LEDs with light intensity of 0.5 suns, 0.75 suns, and 1 sun (1 sun=100 mW·cm^{-2}).

Characterization

Transmission electron microscopy (TEM) was performed on a FEI, Tf20 (Thermo Fisher Scientific). Energy Dispersive Spectrometry (EDS) elemental maps and representative high-resolution transmission electron micrographs (HRTEM) were

carried out on a 200X, Talos (Thermo Fisher Scientific). Powder X-ray diffraction (XRD) patterns of dried samples were recorded on an Empyrean diffractometer with Cu K α radiation. The particle size distribution of different samples was counted via Nano Measurement (at least 100 particles were included for each sample). The Pd and Ni contents of different samples were measured by an ICP-MS (Aurora M90, Jenoptik). XPS was performed using a Thermo Fischer ESCALAB 250Xi spectrometer with an Al Ka X-ray source operating at 15 kV. Absorption spectra were obtained using a Lambda 750 UV/VIS/NIR spectrometer from Perkin Elmer.

In situ hard X-ray absorption spectroscopy (In situ hXAS)

The Pt K-edge hXAS spectra were collected in transmission mode at beamline 11B of the Shanghai Synchrotron Radiation Facility (SSRF, China). Specifically, for hXAS measurements, each sample was sealed within Kapton tape to preclude exposure to air. The final 2D images were achieved through a data process involving normalization to the beam flux and collection time, integration, and combination. The in situ hXAS measurements was performed in a similar manner as described above, except that 100 mW·cm^{-2} of visible band radiation was provided externally.

Computational Methods for partial charges

The p-nitrophenol and p-aminophenol molecular ball-and-stick models were imported into GAUSSIAN software for Hirshfeld charge distribution analysis. The job type was chosen as Optimization and Frequency, and the calculation method was ground state.

Finite difference time domain (FDTD)

The electric field intensity distribution and extinction profile of Pt-Cu alloy are simulated using finite difference time domain (FDTD). In the simulation, the Pt-Cu alloy is simplified as nanospheres, and the relevant refractive index data are obtained from the CRC model, and the dimensions of the particles are obtained from the TEM data, in which the nanospheres' radii are 1.5 nm, and the spacing between the particles is 0 nm and 10 nm, respectively. The light source used in the simulation is a TFSF (total-field scattering field) light source, and a three-dimensional simulation is used for the electric field strength simulation, with the light source incident from top to bottom. In the extinction coefficient simulation, the alloy arrangement is simplified to a particle array, and the light source is set directly in front of the array, and the final extinction efficiency obtained is the result of the extinction cross-section normalized by the geometric area.

In situ diffuse reflection infrared Fourier transform spectroscopy (DRIFTS)

In situ DRIFTS experiments were performed using a FTIR spectrometer (Thermo Nicolet iS50). The catalyst was placed in a 20 mL·min^{-1} Ar flow at room temperature for 1 hour and then the inlet flow was switched to 20 mL·min^{-1} CO for 30 min. Finally, 20 mL·min^{-1} Ar purged the catalyst for 30 min. Spectrum (64 scans) were collected with a resolution of 4 cm^{-1}.
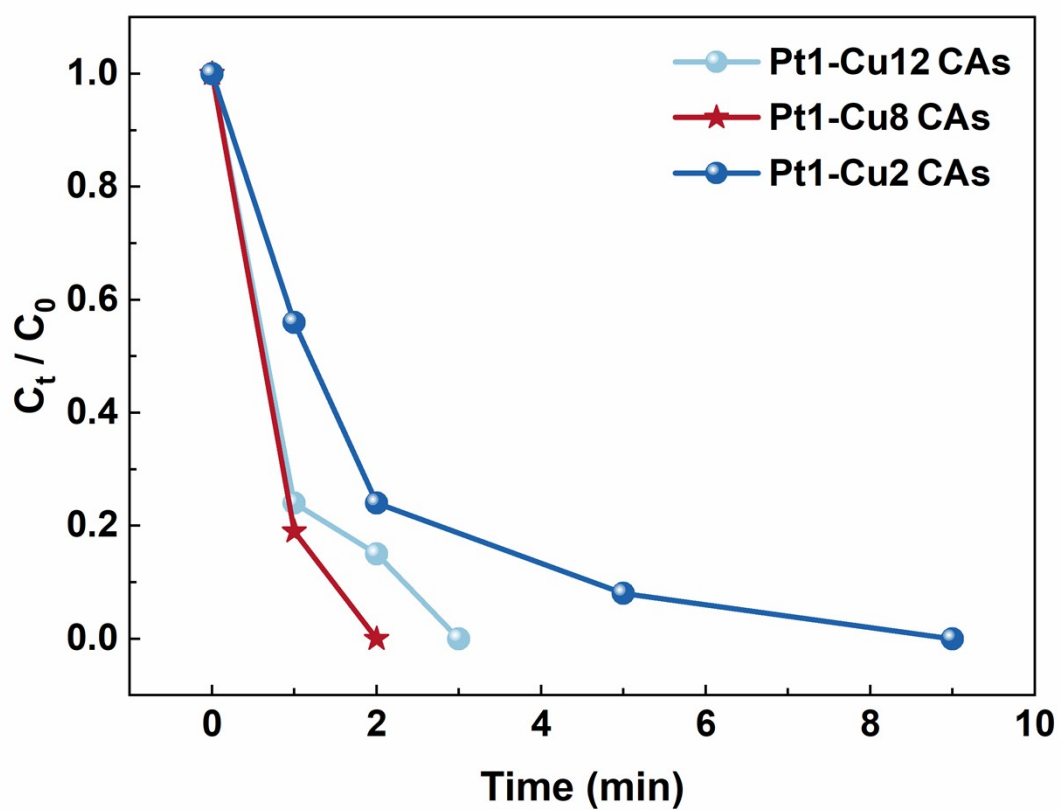
Supplementary Figures
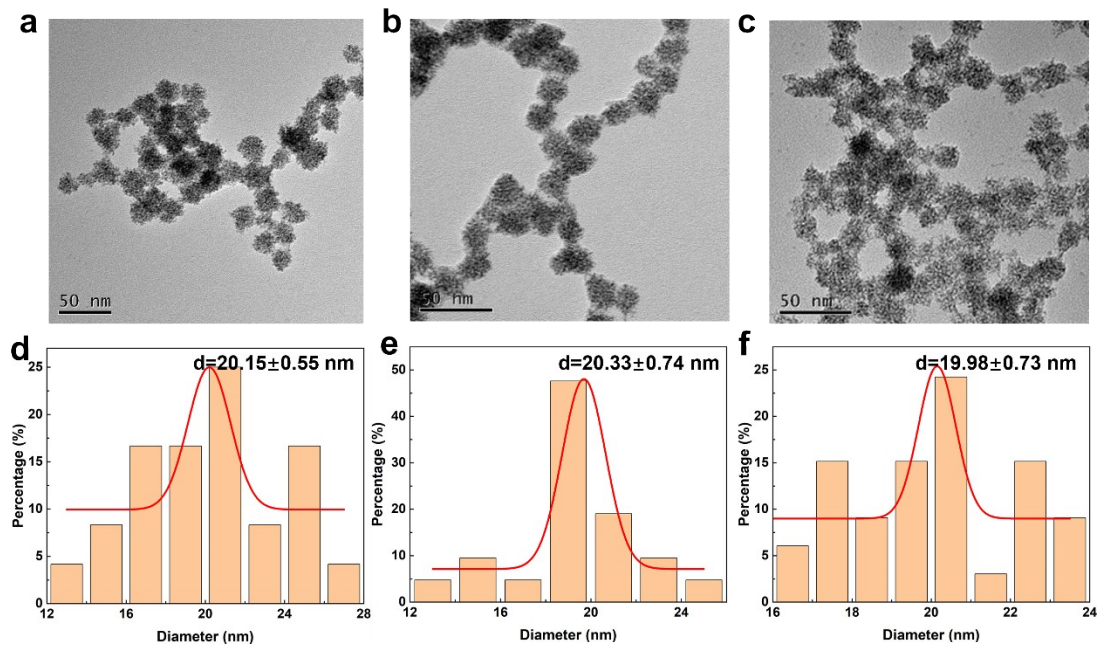
Fig. S1 TEM images and particle size distribution of (a, d) Pt1-Cu2 CAs, (b, e) Pt1-Cu8 CAs and (c, f) Pt1-Cu12 CAs.
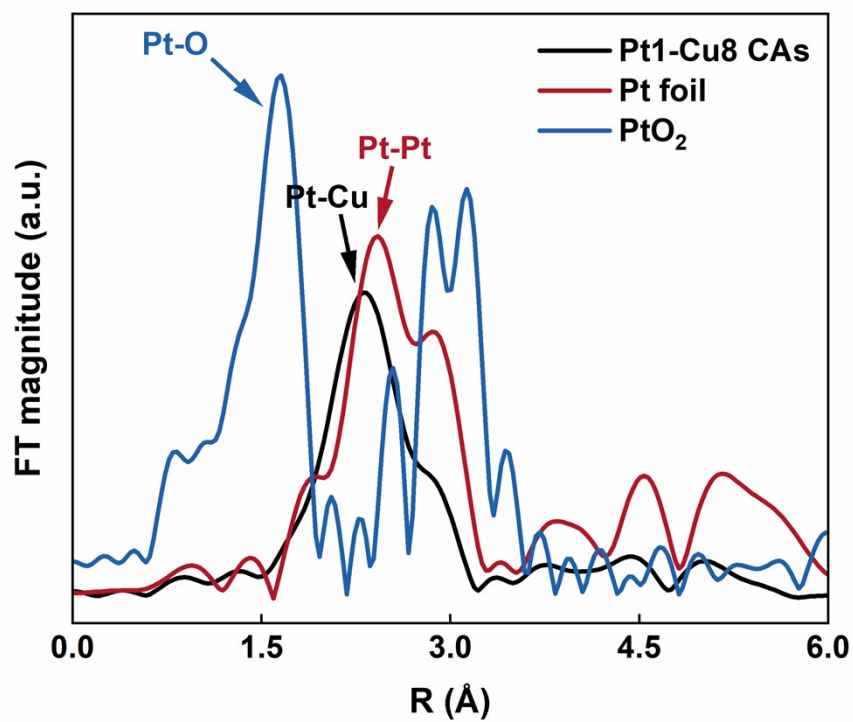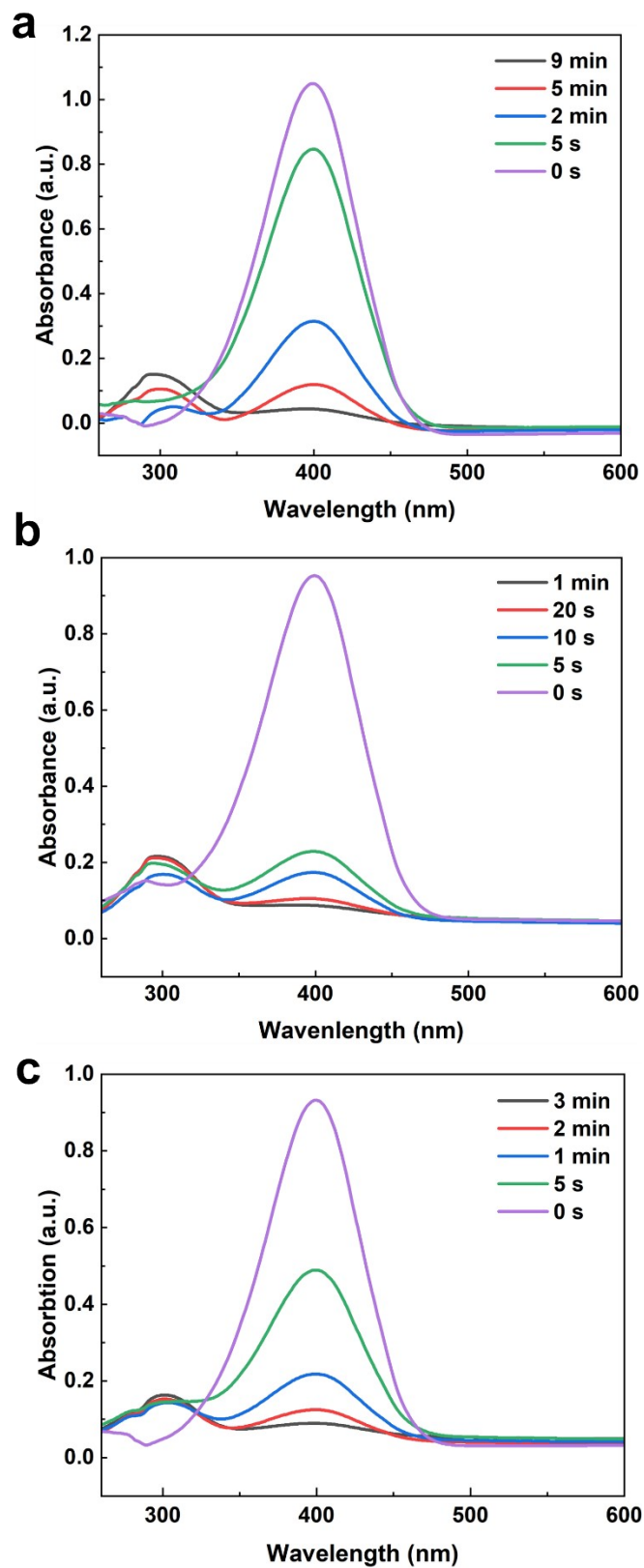
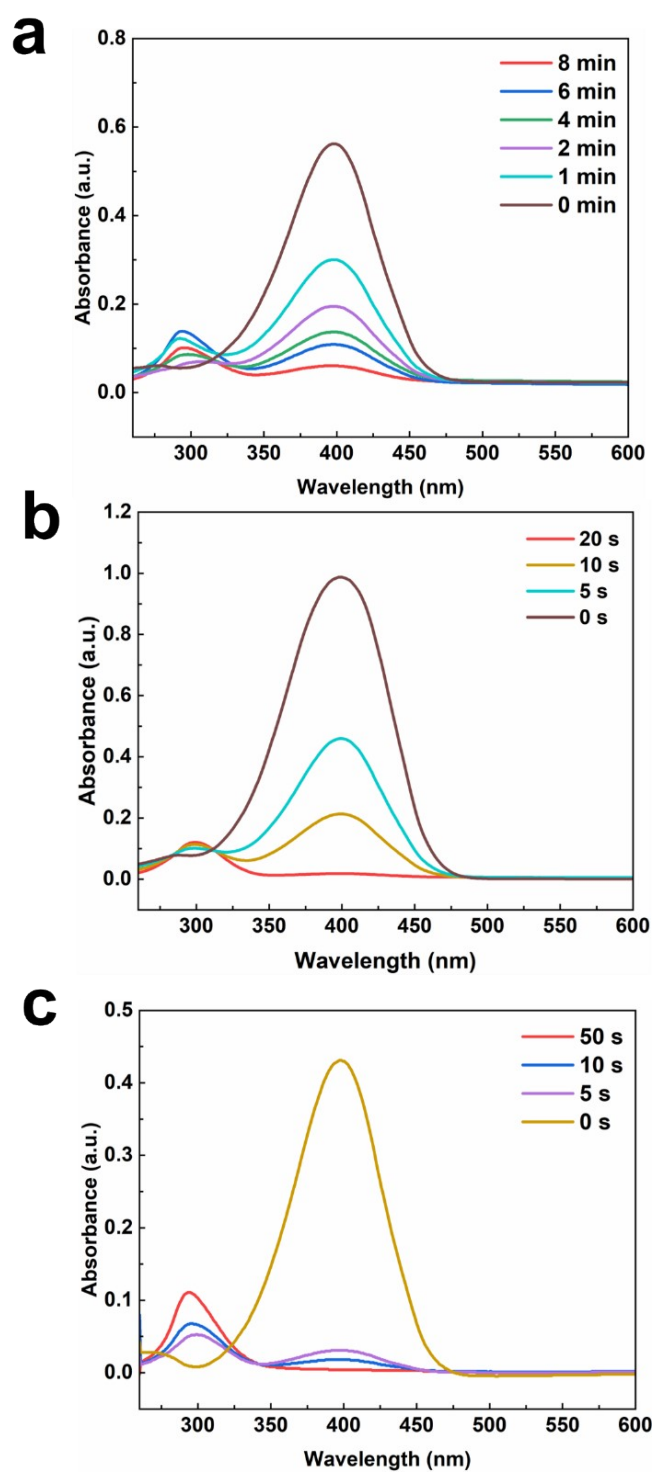**Fig. S2** Curves of the EXAFS spectra at the Pt K-edge for Pt1-Cu8 CAs.

Fig. S3 Time-dependent p-NP conversion of Pt-Cu CAs with different Pt/Cu ratios (Pt1-Cu2, Pt1-Cu8, and Pt1-Cu12).
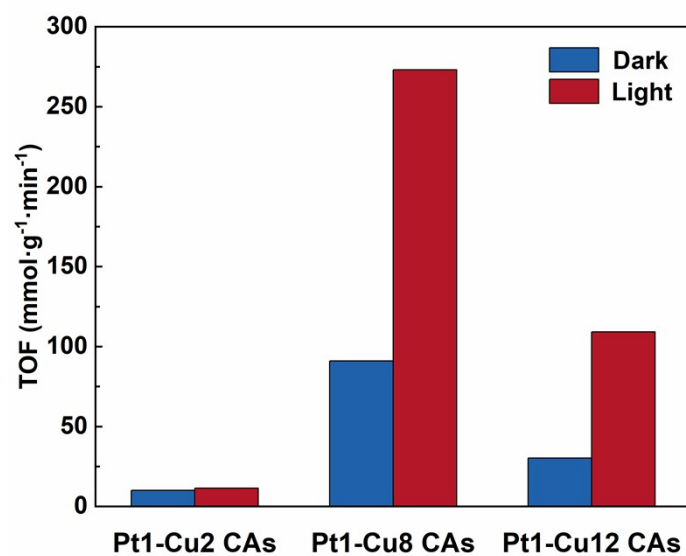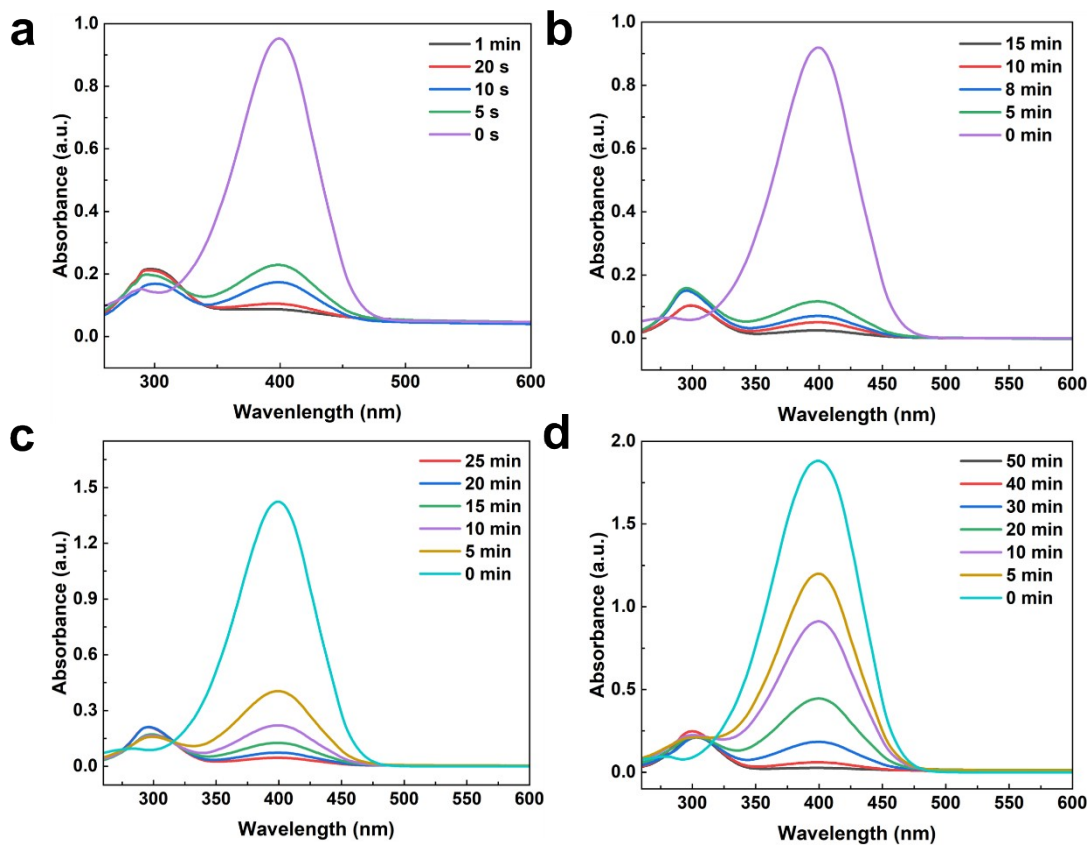
Fig. S4 UV−vis absorption spectra of the reduction of p-NP over Pt-Cu CAs with different Pt/Cu ratios in dark for (a) Pt1-Cu2, (b) Pt1-Cu8, and (c) and Pt1-Cu12. The initial concentration of p-NP is 10^{-4} mol·L^{-1}.
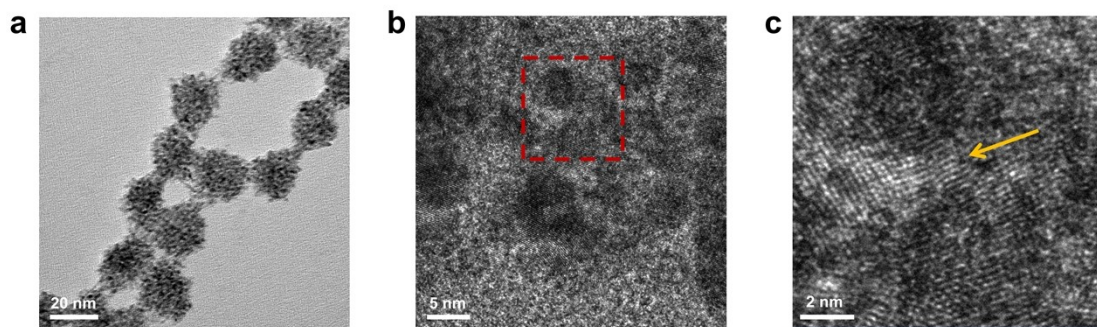
Fig. S5 UV−vis absorption spectra of the reduction of p-NP over Pt-Cu CAs with different Pt/Cu ratios under 100 mW cm^2 light for (a) Pt1-Cu2, (b) Pt1-Cu8, and (c) and Pt1-Cu12. The initial concentration of p-NP is 10^{-4} mol·L^{-1}.

Fig. S6 Comparison of catalytic activity of Pt1-Cu2 CAs, Pt1-Cu8 CAs, and Pt1-Cu12 CAs under dark and light conditions. The initial concentration of p-NP is 10^{-4} mol·L^{-1}. The light intensity is 100 mW cm^2.
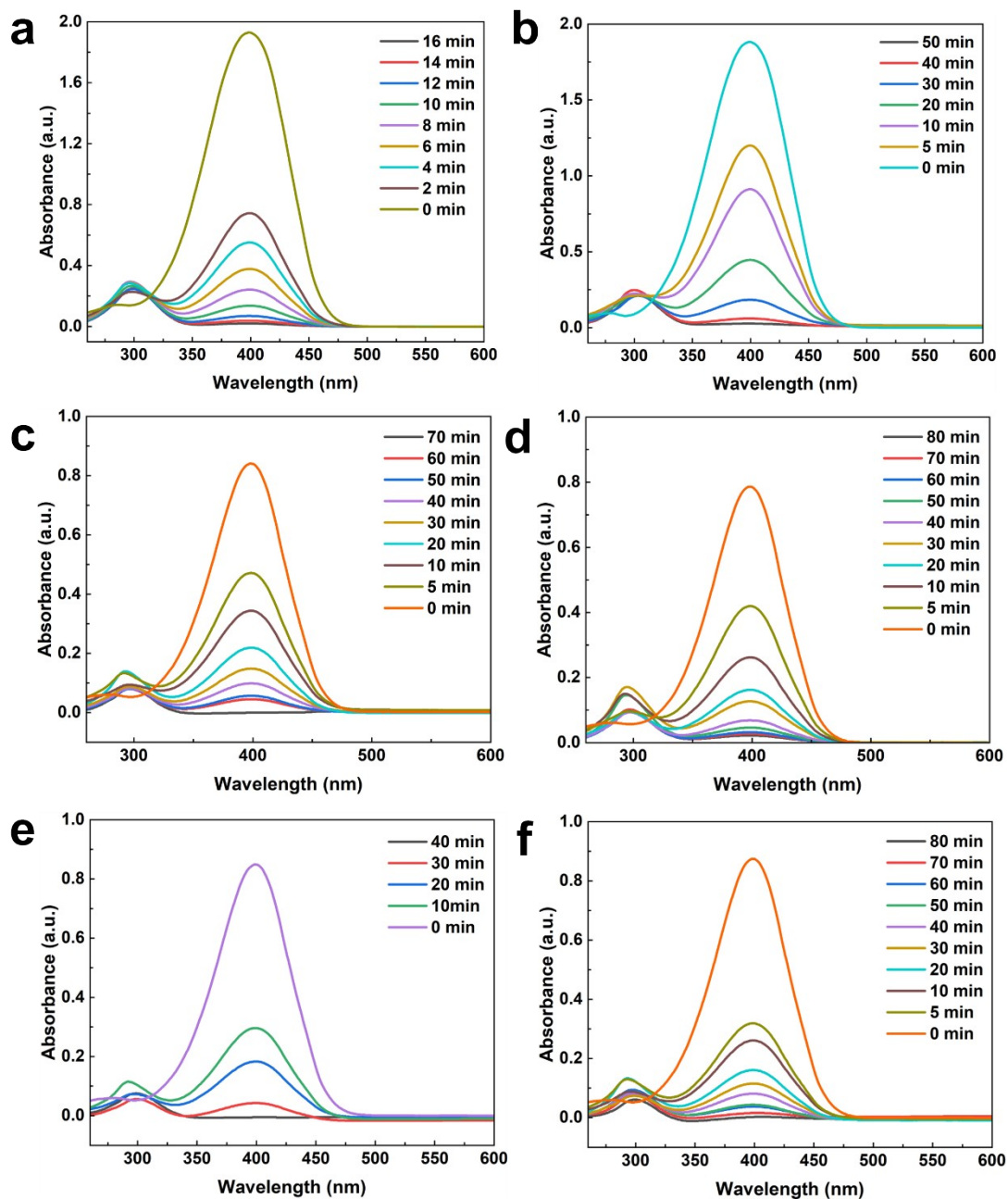
Fig. S7 UV−vis absorption spectra of the reduction of p-NP over Pt1-Cu8 CAs with different concentrations of p-NP for (a) 1×10^{-4} mol·L^{-1}, (b) 5×10^{-4} mol·L^{-1}, (c) 8×10^{-4} mol·L^{-1}, and (d) 1×10^{-3} mol·L^{-1}.

Fig. S8 TEM (a) and HRTEM (b,c) images of Pt1Cu8 CAs after reduction of p-NP.
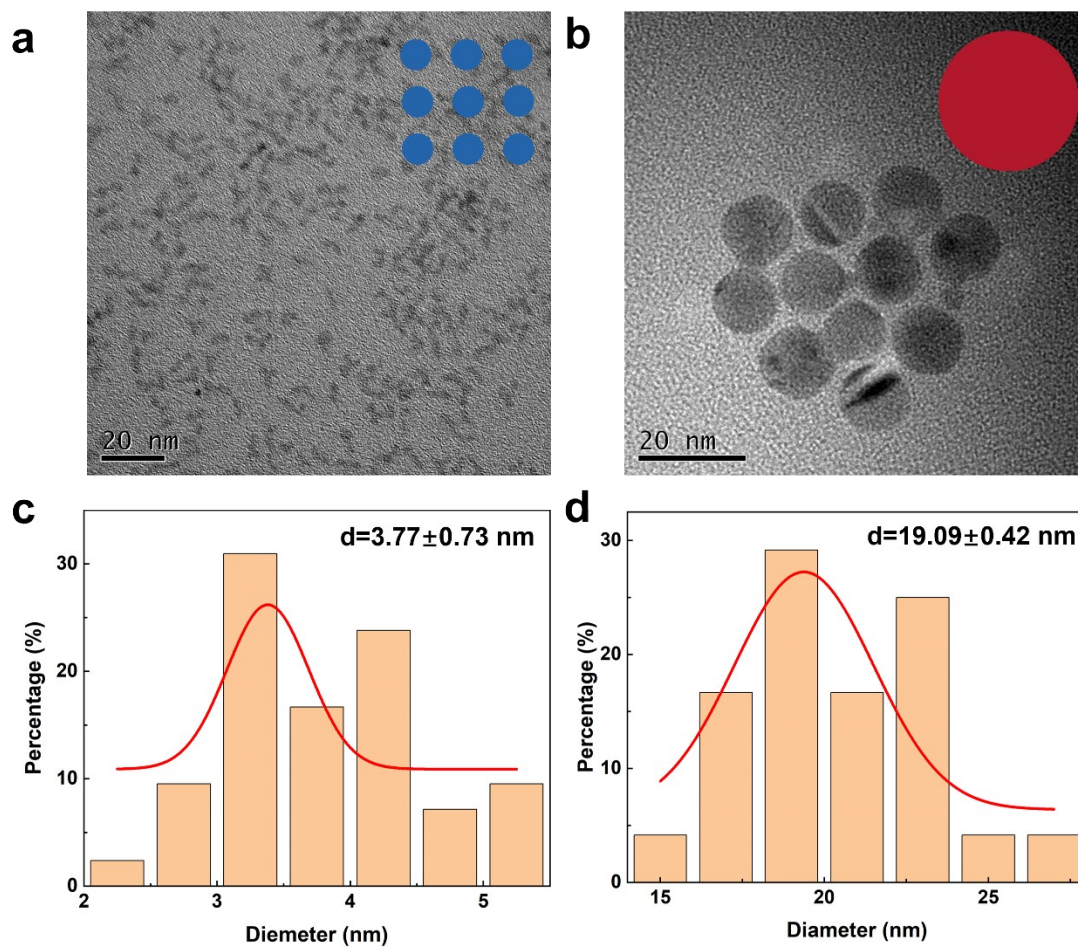
Fig. S9 TEM images and particle size distribution of (a, c) Pt1-Cu8 SPs and (b, d) Pt1-Cu8 LPs.

Fig. S10 UV−vis absorption spectra of the reduction of p-NP over (a-b) Pt1-Cu8 CAs, (c-d) Pt1-Cu8 SPs, and (e-f) Pt1-Cu8 LPs with different shape under 0.1 W cm^{-2} light (left column) and dark conditions (right column).
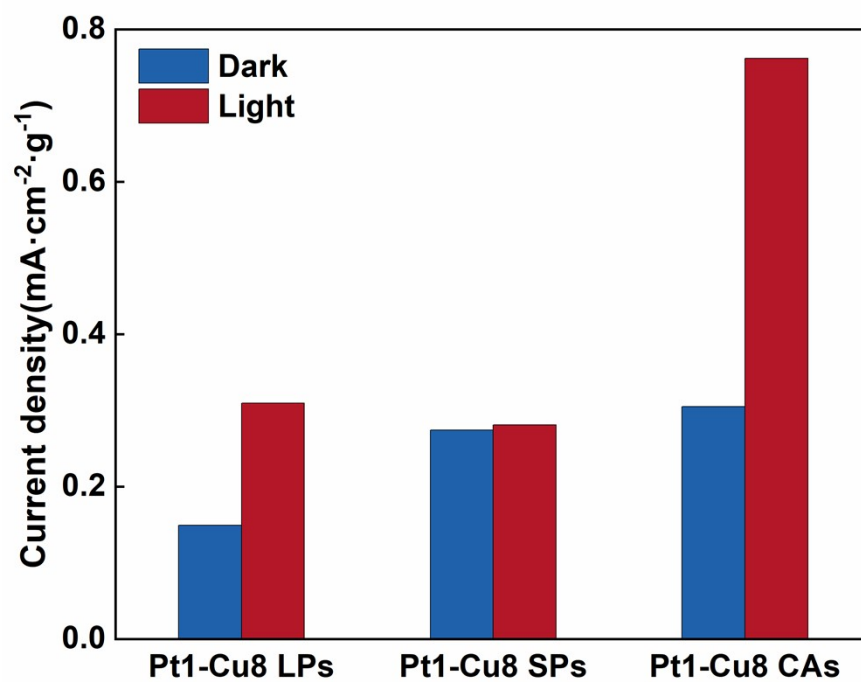
Fig. S11 Comparison of photoelectrochemical activity of Pt1-Cu8 LPs, Pt1-Cu8 SPs, and Pt1-Cu8 CAs under dark and light conditions.
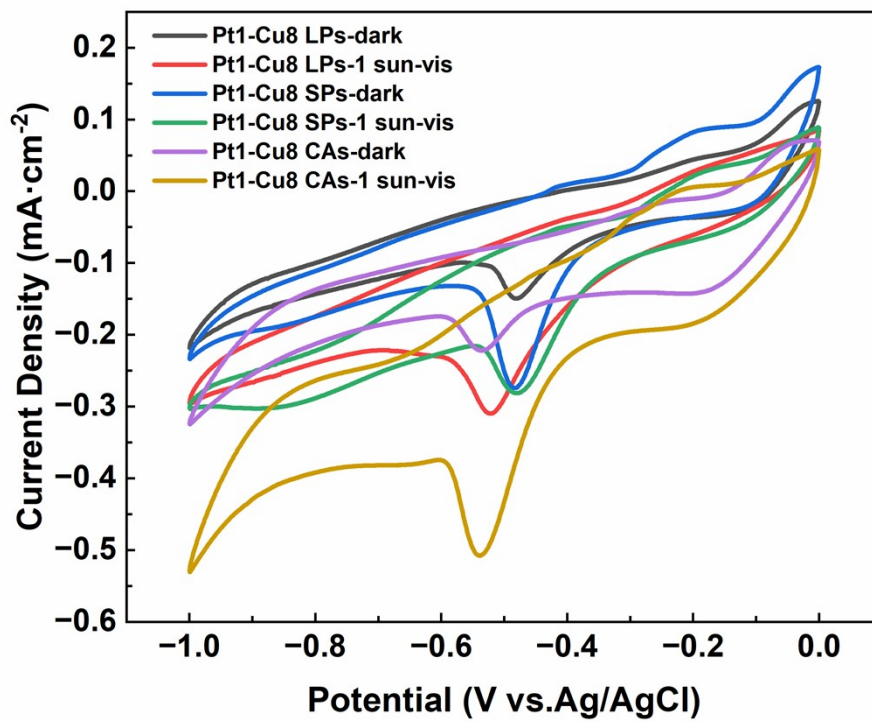
Fig. S12 CV curves of Pt1-Cu8 LPs, Pt1-Cu8 SPs, and Pt1-Cu8 CAs under dark and light conditions.
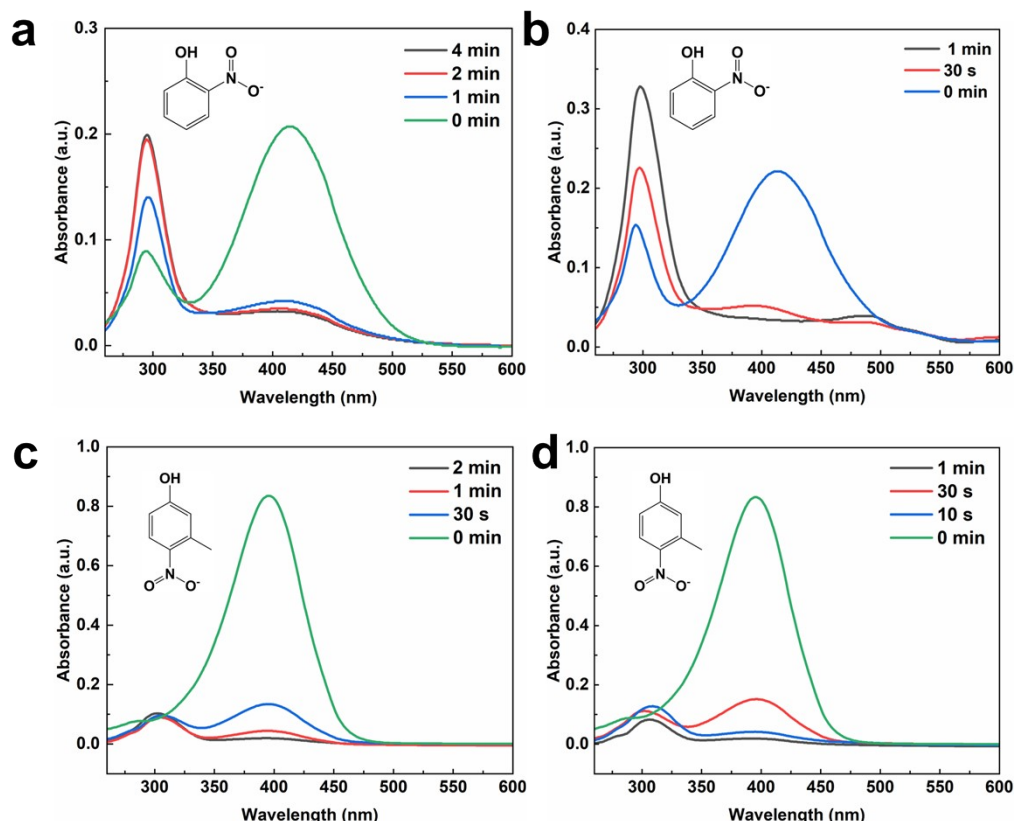
Fig. S13 UV−vis absorption spectra of the reduction of 2-nitrophenol over Pt1-Cu8 CAs under (a) dark and (b) light (1 sun) conditions. UV−vis absorption spectra of the reduction of 3-Methyl-4-nitrophenol over Pt1-Cu8 CAs under (c) dark and (d) light (1 sun) conditions.
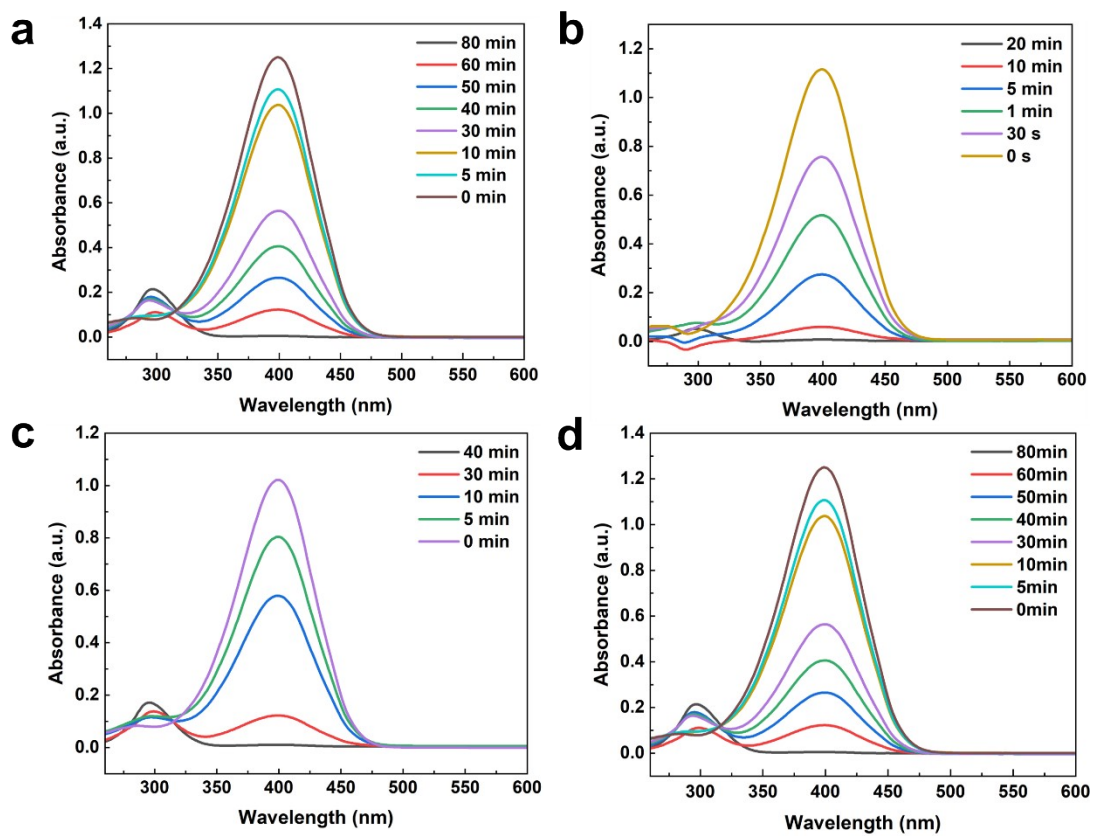
Fig. S14 UV−vis absorption spectra of the reduction of p-NP over Pt1-Cu8 CAs with different light intensity: (a) 3 suns, (b) 2 suns, (c) 1 sun and (d) 0.5 suns.
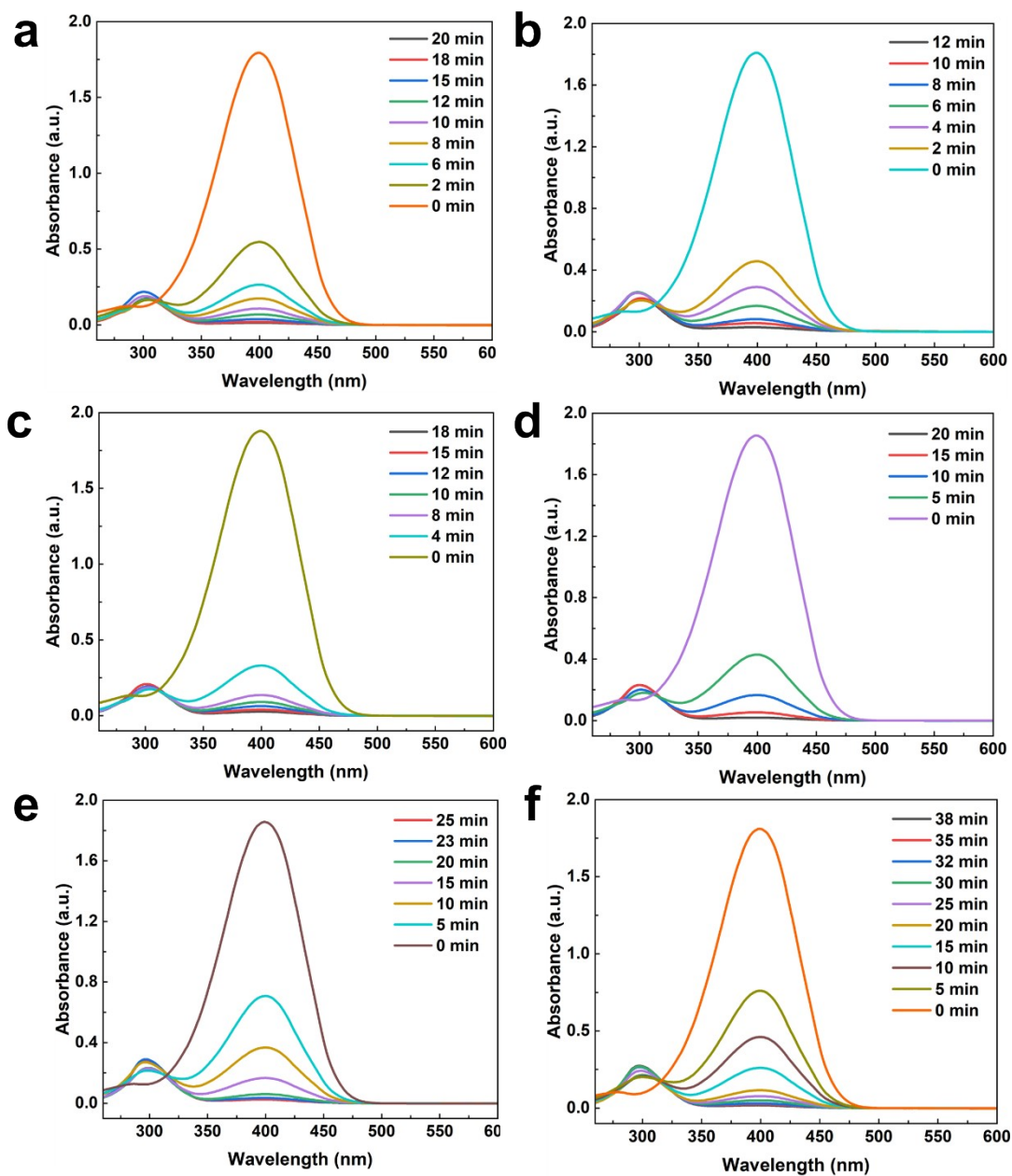
Fig. S15 UV−vis absorption spectra of the reduction of p-NP over Pt1-Cu8 CAs with different light wavelength: (a) 365 nm, (b) 420 nm, (c) 470 nm, (d) 520 nm, (e) 620 nm and (f) 720 nm.
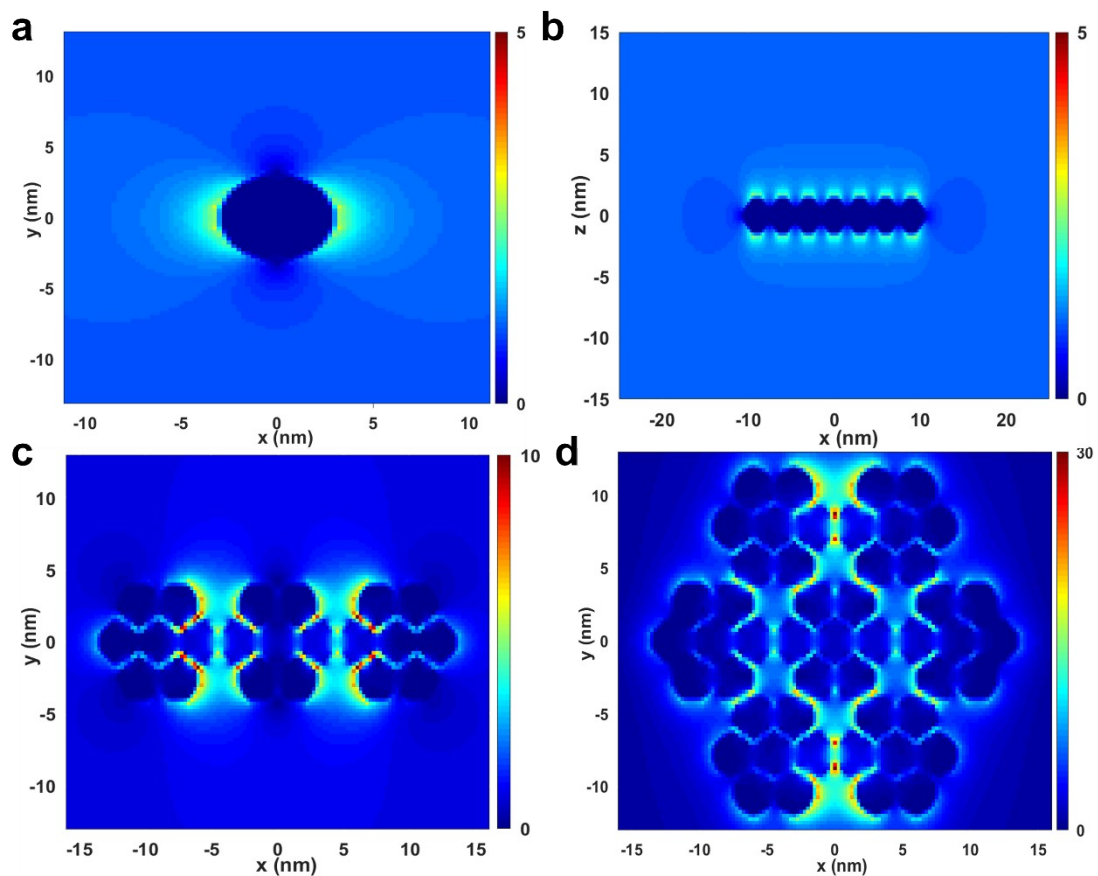
Fig. S16 Simulated electric fields of (a) a single large Pt-Cu alloy nanoparticle, (b) Pt-Cu alloy nanoparticles arranged in a single row, (c) three tightly packed Pt-Cu CAs and (d) five tightly packed Pt-Cu CAs.
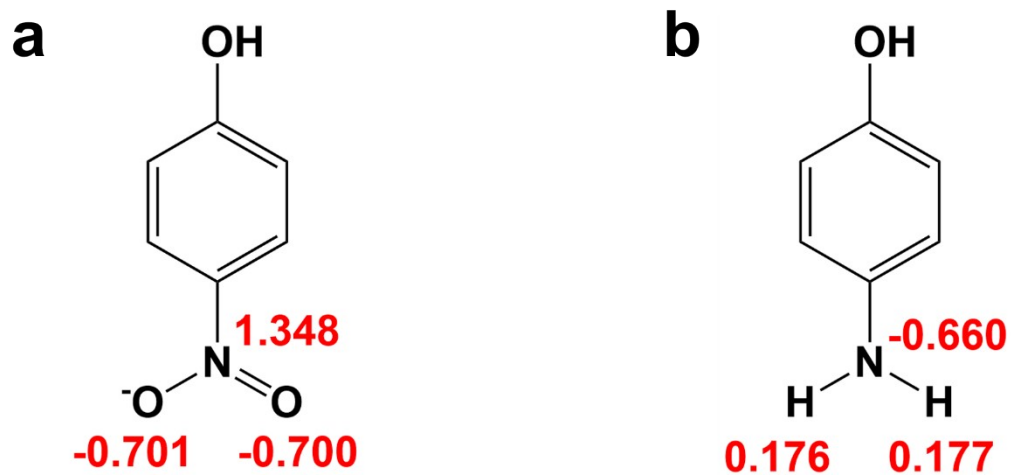
Fig. S17 Hirshfeld charge distribution analysis result of (a) p-NP and (b) p-AP.

Table S1 Comparison of the catalytic activities of some reported catalysts for p-NP reduction.

Number	Catalysts	Reductant	Reaction time (min)	Conversion (%)	Metal content (wt%)	TOF (mmol·g^{-1}·min^{-1})	Concentration (mol·L^{-1})	Irradiation	Ref.
1	Pt1-Cu8 CAs	NaBH$_4$	1	~100	65.6	91.46	1.00×10^(-4)	N	This work
2	Pt1-Cu8 CAs	NaBH$_4$	80	~100	65.6	4.125	0.003	Y-0.5 suns	This work
3	Pt1-Cu8 CAs	NaBH$_4$	14	~100	65.6	23.6	0.003	Y-3 suns	This work
4	Pt1-Cu8 CAs	NaBH$_4$	40	~100	65.6	8.25	0.003	Y-1 sun	This work
5	Pt1-Cu8 CAs	NaBH$_4$	20	~100	65.6	17.5	0.003	Y-2 suns	This work
6	Pt1-Cu8 CAs	NaBH$_4$	0.33	~100	65.6	273	1.00×10^(-4)	Y-1 sun	This work
7	Pt1-Cu8 CAs	NaBH$_4$	16	~100	65.6	9.53	0.001	Y-1 sun	This work
8	Pt1-Cu8 CAs	NaBH$_4$	50	~100	65.6	3.05	0.001	N	This work
9	Cu$_2$O @ZIF-8	NaBH$_4$	14	~99	20.7	0.7	1.25×10^(-4)	N	1
10	Nanoscale zerovalent iron	NaBH$_4$	20	~100	100	1.43	0.001	N	2
11	Cu/C	NaBH$_4$	2.5	~100	49.1	1.28	1.25×10^(-4)	N	3
12	Cu/α-Fe$_2$O$_3$	NaBH$_4$	0.83	~100	20	0.9	5.00×10^(-5)	N	4
13	Faceted Cu NCs	NaBH$_4$	3	~100	100	0.59	1.00×10^(-4)	N	5
14	Ni/C	NaBH$_4$	3	~100	45.8	1.97	1.00×10^(-4)	N	6
15	Co$_{0.5}$Ni$_{0.5}$/C-600	NaBH$_4$	4	~100	39.29	3.82	1.00×10^(-4)	N	7
16	Ni/Ni$_3$S$_2$ @C	NaBH$_4$	6	~99.9	39.37	3	1.20×10^(-4)	N	8
17	CdS/NS- rGO	NaBH$_4$	6	~100	3.89	1.54	1.40×10^(-4)	N	9

18	MoS$_2$/SnO$_2$	NaBH$_4$	13	~100	67	0.02	1.00×10^{-4}	N	10
19	Au NPs	NaBH$_4$	2	~100	100	2.91	0.002	N	11
20	Au/graphene	NaBH$_4$	12	~100	2.4	1.76	1.00×10^{-4}	N	12
21	AuNP-SPEG$_{30K}$	NaBH$_4$	0.4±0.1	~100	65	0.74	2.00×10^{-4}	N	13
22	Au @TpPa-1	NaBH$_4$	18	~100	1.2	0.63	1.80×10^{-4}	N	14
23	Au/g-C$_3$N$_4$	NaBH$_4$	8.4±0.1	~100	5.56	8.08	7.00×10^{-5}	N	15
24	Pd @Ru nanosheets	NaBH$_4$	8	~100	100	3.4	1.50×10^{-4}	N	16
25	NCT @Pd	NaBH$_4$	0.67	~100	0.324	27.8	2.00×10^{-4}	N	17
26	AgPd NC/rGO	NaBH$_4$	3	~95.8	76.9	2.9	7.00×10^{-4}	N	18
27	Ag NPs/SiNSs	NaBH$_4$	0.67	~100	3.26	27.5	1.20×10^{-4}	N	19
28	AC-Ag	NaBH$_4$	6	~100	2.7	9.26	1.00×10^{-4}	N	20
29	Ag/Fe oxide	NaBH$_4$	28	~100	8.35	8.34	7.95×10^{-5}	N	21
30	GO-DAP- Ag NPs	NaBH$_4$	12	~100	20	0.08	1.00×10^{-4}	N	22
31	Pt @Ag	NaBH$_4$	8	~100	100	0.67	1.00×10^{-4}	N	23
32	MSNCs-MH2-Ag	NaBH$_4$	4.83	~100	15.43	20.13	1.20×10^{-4}	N	24
33	PtRh	NaBH$_4$	20	~94.02	3.49	1	8.00×10^{-4}	N	25

References

1. B. Li, J.-G. Ma and P. Cheng, *Angew. Chem. Int. Ed.*, 2018, 57, 6834–6837.

2. S. Bae, S. Gim, H. Kim and K. Hanna, *Appl. Catal. B*, 2016, 182, 541–549.

3. Y. Bai, Q. Wang, C. Du, T. Bu, Y. Liu, X. Sun, W. Luo, R. Li, Y. Zhao, X. Zheng and L. Wang, *J. Colloid Interface Sci.*, 2019, 553, 768–777.

4. A. Elfiad, F. Galli, L. M. Boukhobza, A. Djadoun and D. C. Boffito, *J. Environ*, 2020, 8, 104214.

5. P. Zhang, Y. Sui, G. Xiao, Y. Wang, C. Wang, B. Liu, G. Zou and B. Zou, *J. Mater. Chem. A*, 2013, 1, 1632–1638.

6. G. Wu, X. Liang, H. Zhang, L. Zhang, F. Yue, J. Wang and X. Su, *Catal. Commun.*, 2016, 79, 63–67.

7. Y. Zhao, B. Cao, X. Wang, X. Wang, M. Al-Mamun, H. Zhao, J. Wang, Y. Zheng and X. Su, *J. Environ*, 2018, 6, 5239–5248.

8. X. Wang, J. Lu, Y. Zhao, X. Wang, Z. Lin, X. Liu, R. Wu, C. Yang and X. Su, *ChemCatChem*, 2018, 10, 4143–4153.

9. W. Han, L. Chen, W. Song, S. Wang, X. Fan, Y. Li, F. Zhang, G. Zhang and W. Peng, *Appl. Catal. B*, 2018, 236, 212–221.

10. X.-Q. Qiao, Z.-W. Zhang, D.-F. Hou, D.-S. Li, Y. Liu, Y.-Q. Lan, J. Zhang, P. Feng and X. Bu, *ACS Sustain. Chem. Eng.*, 2018, 6, 12375–12384.

11. W. Shen, Y. Qu, X. Pei, S. Li, S. You, J. Wang, Z. Zhang and J. Zhou, *J. Hazard. Mater.*, 2017, 321, 299–306.

12. J. Li, C. Liu and Y. Liu, *J. Mater. Chem.*, 2012, 22, 8426.

13. S. M. Ansar and C. L. Kitchens, *ACS Catal.*, 2016, 6, 5553–5560.

14. P. Pachfule, S. Kandambeth, D. D. Díaz and R. Banerjee, *Chem. Commun.*, 2014, 50, 3169–3172.

15. Y. Fu, T. Huang, B. Jia, J. Zhu and X. Wang, *Appl. Catal. B*, 2017, 202, 430–437.

16. Z. Zhang, Y. Liu, B. Chen, Y. Gong, L. Gu, Z. Fan, N. Yang, Z. Lai, Y. Chen, J. Wang, Y. Huang, M. Sindoro, W. Niu, B. Li, Y. Zong, Y. Yang, X. Huang, F. Huo, W. Huang and H. Zhang, *Adv. Mater.*, 2016, 28, 10282–10286.

17. X. Duan, M. Xiao, S. Liang, Z. Zhang, Y. Zeng, J. Xi and S. Wang, *Carbon*, 2017, 119, 326–331.

18. Z. Xy, L. Zs, F. Jj, Y. Px, Z. L, C. Jr and W. Aj, *J. Colloid Interface Sci.*, 2018, 01, 047.

19. Z. Yan, L. Fu, X. Zuo and H. Yang, *Appl. Catal. B*, 2018, 226, 23–30.

20. L. Shui, G. Zhang, B. Hu, X. Chen, M. Jin, G. Zhou, N. Li, M. Muhler and B. Peng, *J. Energy Chem.*, 2019, 36, 37–46.

21. J.-R. Chiou, B.-H. Lai, K.-C. Hsu and D.-H. Chen, *J. Mater. Chem.*, 2013, 248–249, 394–400.

22. J. Nimita Jebaranjitham, C. Mageshwari, R. Saravanan and N. Mu, *Composites Part B*, 2019, 171, 302–309.

23. Z.-S. Lv, X.-Y. Zhu, H.-B. Meng, J.-J. Feng and A.-J. Wang, *J. Colloid Interface Sci.*, 2019, 538, 349–356.

24. Cui, G.; Sun, Z.; Li, H.; Liu, X.; Liu, Y.; Tian, Y.; Yan, S. *J. Mater. Chem. A*, 2016, 4, 1771–1783.

25. Q. Yan, X.-Y. Wang, J.-J. Feng, L.-P. Mei and A.-J. Wang, *J. Colloid Interface Sci.*, 2021, 582, 701–710.